ARTICLES
https://doi.org/10.1038/s41566-019-0556-6
nature photonics

4H-silicon-carbide-on-insulator for integrated quantum and nonlinear photonics

Daniil M. Lukin[1,3], Constantin Dory[1,3], Melissa A. Guidry[1,3], Ki Youl Yang[1], Sattwik Deb Mishra[1], Rahul Trivedi[1], Marina Radulaski[1,2], Shuo Sun[1], Dries Vercruysse[1], Geun Ho Ahn[1] and Jelena Vučković[1*]

Optical quantum information processing will require highly efficient photonic circuits to connect quantum nodes on-chip and across long distances. This entails the efficient integration of optically addressable qubits into photonic circuits, as well as quantum frequency conversion to the telecommunications band. 4H-silicon carbide (4H-SiC) offers unique potential for on-chip quantum photonics, as it hosts a variety of promising colour centres and has a strong second-order optical nonlinearity. Here, we demonstrate within a single, monolithic platform the strong enhancement of emission from a colour centre and efficient optical frequency conversion. We develop a fabrication process for thin films of 4H-SiC, which are compatible with industry-standard, CMOS nanofabrication. This work provides a viable route towards industry-compatible, scalable colour-centre-based quantum technologies, including the monolithic generation and frequency conversion of quantum light on-chip.

Silicon carbide—specifically the 4H polytype—is gaining traction as a viable platform for the realization of spin-based quantum technologies, as it hosts a variety of optically addressable defects[1] (that is, colour centres) with long spin coherence times[2–4]. Colour centres like the silicon vacancy (V_{Si})[5], the divacancy (V_CV_{Si})[6] and the nitrogen vacancy (NV)[7] are under experimental and theoretical investigation for applications in solid-state quantum information processing[8–13] and sensing[14,15]. Rapid progress in on-demand, site-controlled single defect generation in 4H-SiC, using a variety of techniques including proton beam writing[16], masked ion implantation[17] and laser annealing[18], promises future scalability of colour-centre-qubit arrays. Thus, SiC has emerged as an alternative to diamond, the current leading platform for colour-centre-based quantum technologies[19–21]. Unique to SiC, however, is the combination of a strong second-order optical nonlinearity[22,23], high thermal conductivity[24], wide bandgap and piezoelectric response[25], which enables integrated quantum transduction and quantum frequency conversion. To realize such applications, advances in quantum-compatible integrated SiC photonics are necessary.

A tried-and-true approach for the development of integrated photonic circuits comprises the use of thin films. Silicon wafers have been widely available since the 1970s, but it was not until the commercialization of the single-crystal silicon-on-insulator (SOI) platform in the 2000s that integrated silicon photonics took off[26]. High-quality crystalline SiC has been commercially available for decades as a result of investment by the semiconductor industry. However, it remains an outstanding challenge to demonstrate thin films with the crystal integrity of sublimation- or homoepitaxially-grown bulk crystal, a critical requirement for scalable quantum photonic architectures. Consequently, although classical photonics devices have been fabricated in thin-film SiC[27–29], all realizations of nanophotonic devices compatible with high-quality colour centres have utilized bulk crystal carving techniques[30,31], which limit the device functionality and versatility in integration with other materials.

In this Article, we demonstrate a low-loss 4H-silicon-carbide-on-insulator (4H-SiCOI) photonics platform using a wafer bonding and thinning technique. In contrast with previous approaches[27–29], the fabrication process does not compromise the crystalline integrity of the device layer. This enabled us to show an improvement in quality factor Q by an order of magnitude over previous approaches in 4H-SiC[28,29]. We observe strongly enhanced single colour centres in high-Q photonic crystal (PhC) cavities and design the SiC–SiO_2 interfaces for low background photoluminescence, thus demonstrating that a SiC platform enables industry-compatible fabrication of colour-centre-based quantum photonic devices. Finally, we demonstrate efficient second-order nonlinear frequency conversion in high-Q microring resonators and design an efficient scheme for fully integrated quantum frequency conversion.

High-quality photonics and colour centres in 4H-SiCOI

The process for the fabrication of 4H-SiCOI begins with fusion bonding of bulk 4H-SiC to an oxidized Si handle wafer, followed by thinning and chemical-mechanical polishing (see Methods). The resulting material stack is a layer of 4H-SiC on top of a buried silicon oxide (SiO_2) layer on silicon. The dimensions of the device and the buried oxide layers may be varied arbitrarily, enabling a variety of photonic applications. Although in this work we demonstrate chip-scale 4H-SiCOI, the methodology may also be implemented at the wafer scale, thus suggesting a pathway towards foundry processing of integrated quantum photonic devices based on colour centres.

Using spatially resolved photoluminescence spectroscopy, we observed single colour centres in 4H-SiCOI (Fig. 1a), which had not been possible before in thin-film SiC due to compromised crystal quality. Colour centre characterization was performed after fabricating micropillars via reactive ion etching to improve the photon collection efficiency[32]. The inset of Fig. 1a shows a scanning electron microscopy (SEM) image of a micropillar, while the main panel shows typical spectra of single V1 (h-lattice site) and V2 (k-lattice site) silicon vacancies (V_{Si})[8,10–12]. Measurements

[1]E. L. Ginzton Laboratory, Stanford University, Stanford, CA, USA. [2]Department of Electrical and Computer Engineering, University of California, Davis, CA, USA. [3]These authors contributed equally: Daniil M. Lukin, Constantin Dory, Melissa A. Guidry. *e-mail: jela@stanford.edu

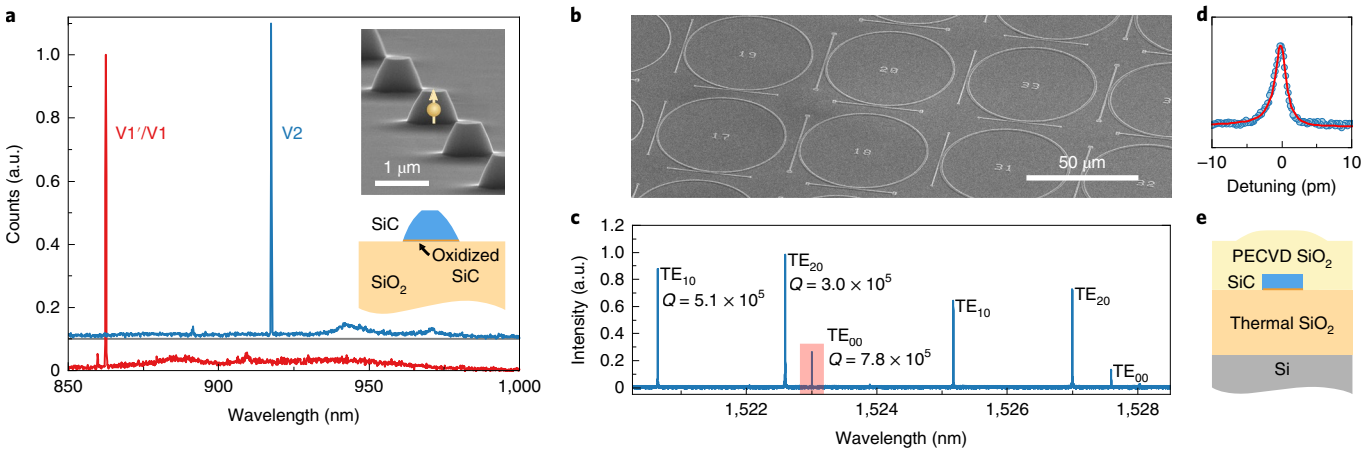

Fig. 1 | Colour centres and photonics in 4H-SiCOI. a, Photoluminescence spectra of colour centres in pillars fabricated in 4H-SiCOI; h-V_{Si} (V1′/V1, red) and k-V_{Si} (V2, blue) show narrow linewidths and low-intensity phonon sidebands. Insets: SEM image of micropillars (top) and corresponding material stack (bottom). **b**, SEM image of an array of 4H-SiCOI ring resonators before SiO_2 encapsulation. **c**, Drop-port spectrum of a ring with diameter of 55 μm, in which three TE mode families can be seen. **d**, A fundamental mode resonance with Q of 7.8×10^5 (highlighted in **c**). **e**, Cross-section of a completed device (dimensions not to scale).

were performed at a temperature of 5 K in a closed-cycle cryostat (Montana Instruments), with above-resonant excitation at 740 nm. The colour centre spectra show weak emission into the phonon sideband and minimal background noise, as reported in bulk 4H-SiC[9,10]. By recording the fraction of micropillars that contain an emitter and estimating the micropillar volume, we arrive at an optically active defect density of 0.1 V_{Si} per μm³. In initial experiments we observed that 4H-SiC is susceptible to strong background noise at the SiC–SiO_2 fusion bond, as well as at interfaces between SiC and the plasma-enhanced chemical vapour-deposited (PECVD) oxide cladding layer. This noise overwhelmed the emission from colour centres and would probably render the platform unusable for quantum applications. However, we found that a 20 nm thermal oxide layer grown on SiC before bonding or PECVD deposition fully eliminated this undesirable photoluminescence, acting as a buffer against optically active formations at the SiC interface. We thus achieved the same low background noise observed in high-purity homoepitaxial bulk crystal[32].

To demonstrate that our 4H-SiCOI approach also enables low-loss SiC photonics, we fabricated microring resonators (Fig. 1b–d). We characterized their optical properties in a two-waveguide drop-port configuration using a fibre-interferometer-calibrated frequency scan (see Methods), as shown in Fig. 1b. Three transverse electric (TE) mode families were observed in rings with diameter of 55 μm, width of 2.5 μm and height of 350 nm. A maximum Q factor of 7.8×10^5 was measured for the fundamental mode, corresponding to a propagation loss of 0.5 dB cm^{-1} (calculated using the simulated effective refractive index of the mode). This is an order of magnitude improvement over the current state of the art in 4H-SiC waveguides, where material absorption is cited as the limiting factor[28,29].

Single silicon vacancy coupled to a nanophotonic resonator

4H-SiC colour centres are promising candidates for optically active solid-state qubits. A critical requirement for multi-qubit spin-based optical quantum information processing is the ability to engineer high-fidelity interactions between a single quantum emitter and light. This can be achieved by placing a quantum emitter into a photonic resonator, thereby enhancing its interaction with light. Enhancement of the dipole–photon interaction in a resonator is quantified by the Purcell factor, which scales as Q/V, where Q is the quality factor and V is the cavity mode volume. Although whispering gallery mode resonators (such as microring resonators) typically have the highest Q among other nanophotonic devices, the microring V is also large (~$10^2(\lambda/n)^3$, where λ is the wavelength in vacuum and n is the refractive index of the material). Thus, to maximize Purcell enhancement, we designed PhC nanobeam cavities with a well-localized TE mode and simulated mode volume of $V = 0.46(\lambda/n)^3$. In fabricated devices, we measured a maximum cavity Q factor of 19,300, corresponding to a Q/V ratio over three times higher than for previous approaches in crystalline SiC[30,31,33,34]. In a recent publication[35], cavities in thin-film SiC in the telecommunications band with a higher Q/V were demonstated using an approach similar to ours, with a design that may offer advantages over nanobeam PhC for colour centre integration.

Although coupling of 4H-SiC colour centre ensembles to nanophotonic resonators has been shown previously[30], to our knowledge, coupling of single colour centres has not been demonstrated. Because of the low intrinsic defect density in the 4H-SiCOI, we introduced additional colour centres into the fabricated nanobeam PhCs via hydrogen ion implantation[16], targeting a density of 3 V_{Si} per cavity (see Methods). Based on the reported polarization of the optical transitions[8,10,11], the primarily in-plane polarized resonator mode is predicted to couple maximally to the V1′ transition and minimally to the V1 and V2 transitions (for a level diagram of h-V_{Si}, see Supplementary Information). For our measurements, we selected a PhC cavity with a Q factor of 14,900 that is blue-shifted from the V1′ transition. Via argon gas condensation, we tuned the cavity resonance at a rate of 15 GHz min^{-1} while continuously acquiring photoluminescence spectra, with excitation (740 nm wavelength) and detection aligned spatially to the centre of the cavity. The zero-phonon lines (ZPLs) of individual V_{Si} become selectively Purcell-enhanced while on resonance with the cavity (individual emitters are labelled 1–4 in Fig. 2b). For further characterization of the coupled emitter–cavity system, we stabilized the cavity on resonance with emitter 2, which has the best spatial overlap with the cavity mode and thus the strongest cavity coupling. We excited the emitter with a 740 nm picosecond pulsed laser and observed that the 6.66 ns off-resonant optical lifetime was reduced to 2.45 ns when the cavity was on resonance (Fig. 2c). The luminescence intensity of the emitter, in turn, was enhanced by a factor of 120 ± 10 (Fig. 2d) compared to off-resonant emission. The complex level structure of V1′ and V1, with many unknown decay rates, does not allow the extraction of the Purcell factor (F)

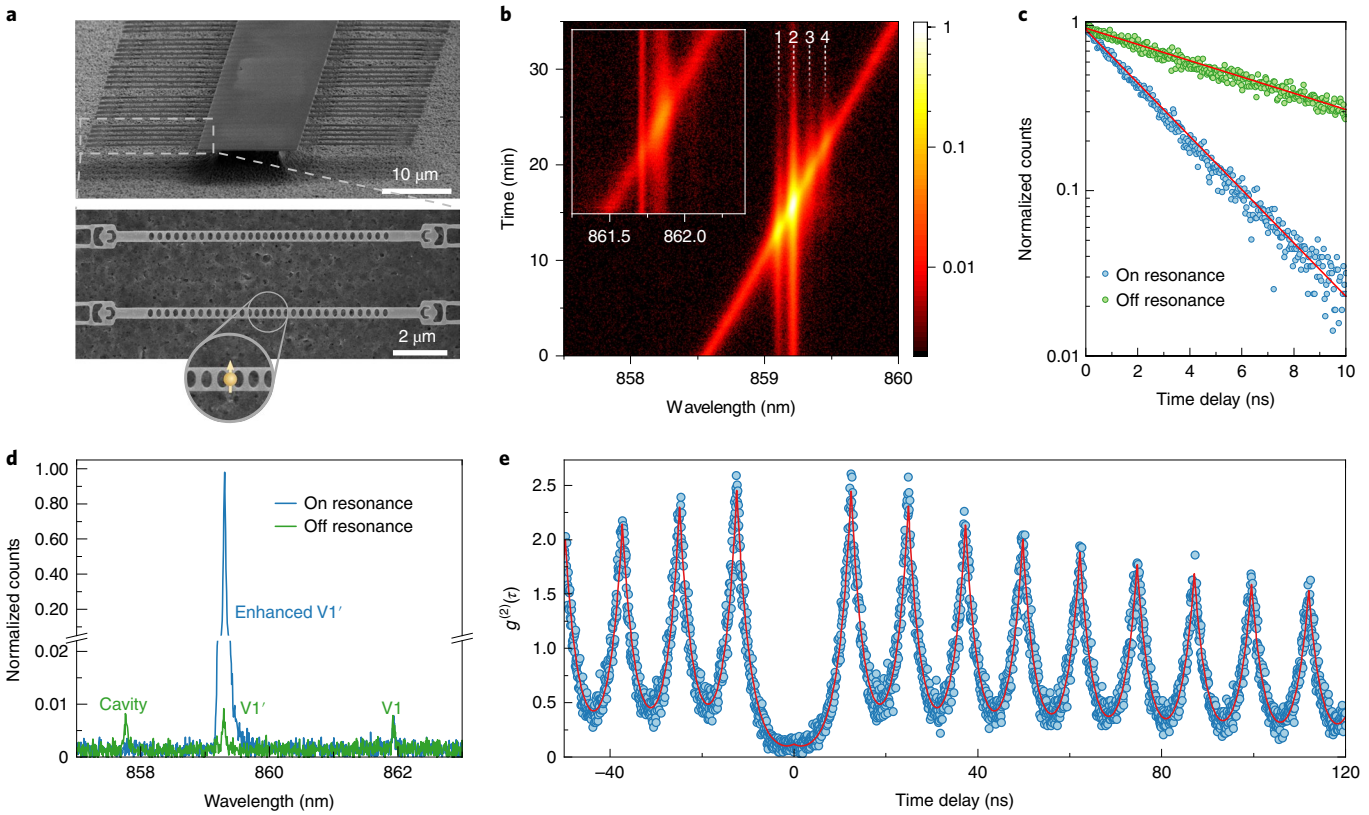

Fig. 2 | Light–matter interaction of a single colour centre with a nanophotonic resonator. a, SEM image of a suspended nanobeam array (top) and enlarged image of the devices from above (bottom). **b**, Stacked spectra obtained while tuning a nanobeam PhC cavity resonance via gas condensation through the V1′. Individual colour centres are indicated by numbers 1–4. Inset: while tuning the cavity resonance through V1, we observe minimal enhancement of V1, which confirms that the dipole moment of the transition is orthogonal to the TE mode of the cavity. **c**, Lifetime measurements with the cavity on and off resonance. Fitted lifetimes are $\tau_{off} = 6.66$ ns and $\tau_{on} = 2.45$ ns. **d**, Spectra extracted from **b** with the cavity off and on resonance with V1′. **e**, Second-order correlation measurement with the cavity on resonance with the V1′ transition of a single emitter, revealing $g^{(2)}(0) = 0.08$.

from the lifetime reduction. A simulation of the cavity fields on and off resonance (see Supplementary Information) suggests that the intensity enhancement is not due to a change in cavity collection efficiency. Thus, although the lower bound on the Purcell factor from the known decay rates of V_{Si} is $F_{min} = 9$, the actual Purcell enhancement is probably much higher (see Supplementary Information). We verified that the cavity is indeed enhancing a single emitter by measuring the two-photon autocorrelation, $g^{(2)}(\tau)$, shown in Fig. 2e, and observing strong anti-bunching at zero time delay. A fit to the data using an effective three-level model (see Supplementary Information) revealed $g^{(2)}(0) = 0.08$, confirming single emitter enhancement.

Nonlinear frequency conversion

Photons are necessary as flying qubits in quantum information processing for long-distance communications and distributed quantum computation. However, the high-transparency window of silica fibres is limited to the 1,300 nm and 1,550 nm infrared bands, whereas nearly all current solid-state qubit candidates emit at other wavelengths. This has motivated a decade of development in quantum frequency conversion (QFC) technology, with the goal of enabling a quantum network that connects nodes operating at different wavelengths and allows long-distance transport of quantum information. The most mature QFC devices utilize the $\chi^{(2)}$ nonlinearity, such as periodically poled lithium niobate waveguides, where single-stage conversion efficiencies of up to 86% have been demonstrated at the single-photon level[36]. The internal quantum efficiency of a device is limited primarily by propagation losses. The total efficiency is further limited by coupling and reflection losses, and such losses may be substantially reduced by integrating the QFC device and the single-photon source on the same chip. The only demonstration so far of nonlinear optics and enhancement of high-quality quantum emitters on a monolithic platform was achieved using quantum dots in GaAs[37]; however, the challenge of achieving low-loss photonics in GaAs has limited progress[38]. Hence, no monolithic material platform integrating quantum photonics and efficient second-order frequency conversion has been demonstrated, to our knowledge, but theoretical proposals have been published[39].

Here, we demonstrate efficient second-harmonic generation (SHG) at sub-milliwatt powers using modal phase-matching in a high-Q microring resonator (Fig. 3a). Towards this end, we designed the dimensions of the ring to induce geometric dispersion to balance the intrinsic material dispersion and allow for phase-matching across a wide frequency separation. To utilize the d_{31} nonlinear term in c-cut 4H-SiC, we designed for phase-matching between the fundamental quasi-TE mode (TE_{00}) at 1,555 nm and a quasi-transverse-magnetic mode (TM_{20}) at 777.5 nm. Finite-element method simulation using anisotropic Sellmeier equations[40] for air-clad 4H-SiC showed that effective refractive index matching is possible between these modes for a waveguide thickness of 350 nm, a waveguide width of 560 nm and a microring radius of 27.5 μm (Fig. 3b). Two bus waveguides were designed to selectively point couple either the pump or second harmonic (SH), each equipped with inverse-designed vertical couplers[41] optimized for the appropriate

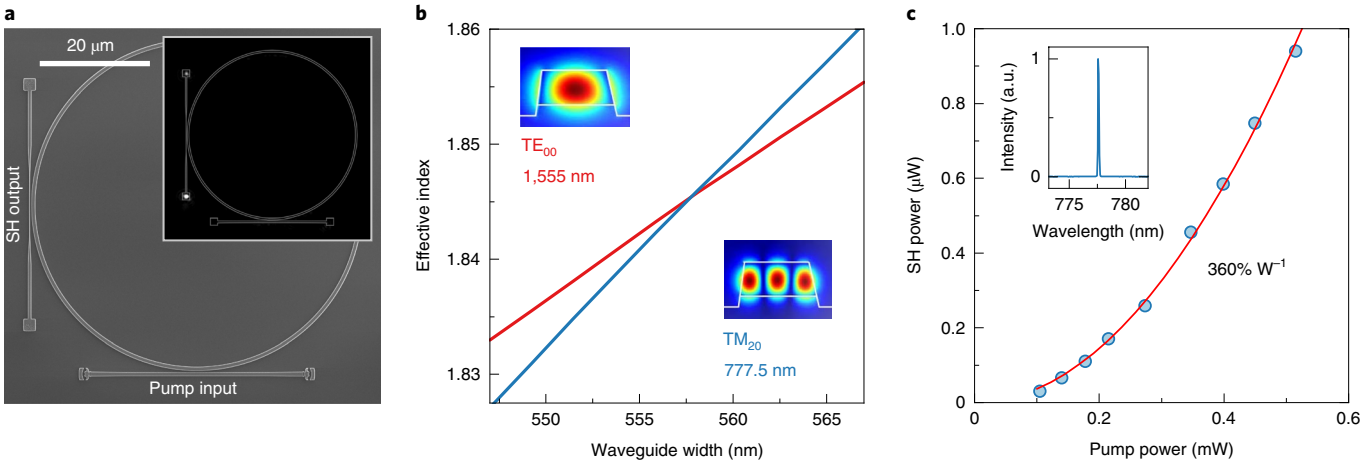

Fig. 3 | Efficient second-order frequency conversion in microring resonators. a, SEM image of a ring resonator designed for SHG. The fundamental TE_{00} mode at 1,555 nm is converted to a TM_{20} mode at 777.5 nm, and coupled out via a single-mode, effective index-matched waveguide. Inset: optical image of the second-harmonic coupled out via an inverse-designed vertical coupler (the ring outline is overlaid for clarity). **b**, Numerical simulation of the phase-matching condition for the 1,555 nm TE_{00} and 777.5 nm TM_{20} modes, demonstrating mode-matching for a waveguide width of 560 nm. Insets: simulated mode profiles. **c**, Dependence of second-harmonic power in the output waveguide on the pump power in the input waveguide. A quadratic fit reveals a conversion efficiency of 360% W^{-1}. Inset: the second-harmonic signal imaged on a spectrometer.

wavelength (Fig. 3a). By means of transmission measurements through each bus waveguide at the respective design wavelength, we measured loaded Q factors of 8×10^4 for the pump at near-critical coupling and 2×10^4 for the second harmonic, undercoupled with a transmission of $T = 0.5$. The devices were designed to be compatible with air-clad inverse-designed vertical couplers. By varying the pump power, we obtained a linear power dependence of the second harmonic on the square of the pump power, as expected in the undepleted pump limit (Fig. 3c). SHG efficiency is defined as the ratio between the generated second-harmonic power in the output waveguide and the square of the pump power in the input waveguide (see Supplementary Information). The efficiency of the SHG process was thus measured to be 360% W^{-1}.

Conclusions and outlook

In this Article, we have demonstrated that 4H-SiC offers unique capabilities for quantum information processing applications. We have introduced a 4H-SiCOI material platform that enables low-loss photonic devices, demonstrated strong enhancement of emission for a single colour centre in a nanophotonic cavity, and designed and fabricated microring resonators for efficient frequency conversion. This work thus provides the first demonstration of strong enhancement of a high-quality quantum emitter and efficient nonlinear optics in the same platform. This positions SiC as a leading candidate for foundry-scale solid-state-qubit-based quantum photonics, with fully integrated, efficient quantum frequency conversion. Using triply resonant microring resonators, a 100% photon conversion efficiency of quantum emitter signal into the telecommunications band can be achieved with 300 μW of 1.93 μm pump laser power (see Supplementary Information). This power requirement may be readily achieved on-chip using high-efficiency inverse-designed vertical couplers[41].

The compatibility of thin-film SiC with industry-standard nanophotonics processing techniques offers the advantage of foundry-based device fabrication, together with complex optical interconnects and multilayer electrical wiring. This makes the 4H-SiC platform promising both in the long run—when robust fabrication protocols will be crucial for large quantum networks—and in the near future, when the low device yields shared by all solid-state quantum photonic platforms may be compensated by device post-selection via photonic circuit reconfigurability. The 4H-SiCOI platform enables, for example, the integration of quantum nodes post-characterization via the fabrication of silicon nitride optical interconnects. Critically, the number of qubits in a network is then limited only by the total number of mutually compatible nodes on a single chip. An example of this technique for a two-qubit device is illustrated in Fig. 4, where two nanobeams coupled to spectrally aligned V1′ transitions of single V_{Si} colour centres are selected, and silicon nitride interconnects are fabricated to realize on-chip spin–spin coupling via Hong–Ou–Mandel photon interference[11]. The versatility of the fabrication platform also enables sensing based on optically detected spin-mechanical resonance in SiC membranes, which holds promise for quantum sensing applications[42,43] as well as studies of fundamental material properties.

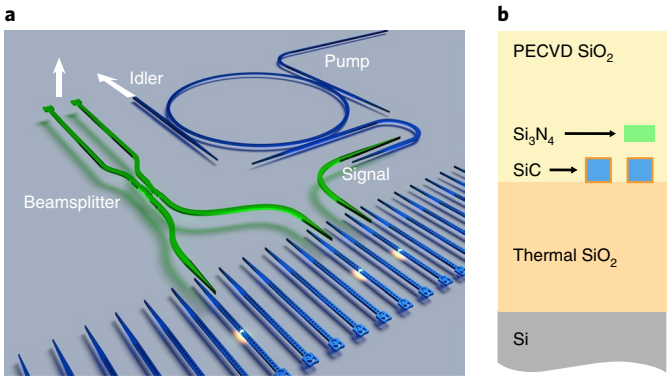

Fig. 4 | A conceptual diagram showing two applications that can be readily implemented with the 4H-SiCOI architecture. a, Left: the realization of a spin–spin entanglement scheme between two emitter–cavity systems. Right: emission from a single V_{Si} is delivered to a high-Q triply resonant ring resonator to achieve frequency conversion to the telecommunication frequencies. Although, for maximum circuit efficiency, it is best to forgo silicon nitride interconnects, this approach may enable short-term multi-qubit integration until near-unity single-qubit yield is attained. **b**, Illustration of the material stack for the proposed platform.

Online content

Any methods, additional references, Nature Research reporting summaries, source data, extended data, supplementary information, acknowledgements, peer review information; details of author contributions and competing interests; and statements of code and data availability are available at https://doi.org/10.1038/s41566-019-0556-6.

Received: 31 March 2019; Accepted: 24 October 2019;
Published online: 2 December 2019

References

1. Lohrmann, A., Johnson, B. C., McCallum, J. C. & Castelletto, S. A review on single photon sources in silicon carbide. *Rep. Prog. Phys.* **80**, 034502 (2017).
2. Simin, D. et al. Locking of electron spin coherence above 20 ms in natural silicon carbide. *Phys. Rev. B* **95**, 161201 (2017).
3. Widmann, M. et al. Coherent control of single spins in silicon carbide at room temperature. *Nat. Mater.* **14**, 164–168 (2015).
4. Koehl, W. F., Buckley, B. B., Heremans, F. J., Calusine, G. & Awschalom, D. D. Room temperature coherent control of defect spin qubits in silicon carbide. *Nature* **479**, 84–87 (2011).
5. Janzén, E. et al. The silicon vacancy in SiC. *Physica B* **404**, 4354–4358 (2009).
6. Son, N. T. et al. Divacancy in 4H-SiC. *Phys. Rev. Lett.* **96**, 055501 (2006).
7. Von Bardeleben, H. J., Cantin, J. L., Rauls, E. & Gerstmann, U. Identification and magneto-optical properties of the NV center in 4H-SiC. *Phys. Rev. B* **92**, 064104 (2015).
8. Nagy, R. et al. High-fidelity spin and optical control of single silicon vacancy centres in silicon carbide. *Nat. Commun.* **10**, 1954 (2019).
9. Nagy, R. et al. Quantum properties of dichroic silicon vacancies in silicon carbide. *Phys. Rev. Appl.* **9**, 034022 (2018).
10. Banks, H. B. et al. Resonant optical spin initialization and readout of single silicon vacancies in 4H-SiC. *Phys. Rev. Appl.* **11**, 024013 (2019).
11. Economou, S. E. & Dev, P. Spin–photon entanglement interfaces in silicon carbide defect centers. *Nanotechnology* **27**, 504001 (2016).
12. Dong, W., Doherty, M. W. & Economou, S. E. Spin polarization through intersystem crossing in the silicon vacancy of silicon carbide. *Phys. Rev. B* **99**, 184102 (2019).
13. Christle, D. J. et al. Isolated spin qubits in SiC with a high-fidelity infrared spin-to-photon interface. *Phys. Rev. X* **7**, 021046 (2017).
14. Von Bardeleben, H. J. et al. NV centers in 3C, 4H and 6H silicon carbide: a variable platform for solid-state qubits and nanosensors. *Phys. Rev. B* **94**, 121202 (2016).
15. Simin, D. et al. All-optical dc nanotesla magnetometry using silicon vacancy fine structure in isotopically purified silicon carbide. *Phys. Rev. X* **6**, 031014 (2016).
16. Kraus, H. et al. Three-dimensional proton beam writing of optically active coherent vacancy spins in silicon carbide. *Nano Lett.* **17**, 2865–2870 (2017).
17. Wang, J. et al. Efficient generation of an array of single silicon-vacancy defects in silicon carbide. *Phys. Rev. Appl.* **7**, 064021 (2017).
18. Chen, Y.-C. et al. Laser writing of scalable single colour centre in silicon carbide. *Nano Lett.* **19**, 2377–2382 (2018).
19. Degen, C. L., Reinhard, F. & Cappellaro, P. Quantum sensing. *Rev. Mod. Phys.* **89**, 035002 (2017).
20. Sipahigil, A. et al. An integrated diamond nanophotonics platform for quantum-optical networks. *Science* **354**, 847–850 (2016).
21. Evans, R. E. et al. Photon-mediated interactions between quantum emitters in a diamond nanocavity. *Science* **362**, 662–665 (2018).
22. Sato, H., Abe, M., Shoji, I., Suda, J. & Kondo, T. Accurate measurements of second-order nonlinear optical coefficients of 6H and 4H silicon carbide. *J. Opt. Soc. Am. B* **26**, 1892–1896 (2009).
23. Martini, F. & Politi, A. Four wave mixing in 3C SiC ring resonators. *Appl. Phys. Lett.* **112**, 251110 (2018).
24. Qian, X., Jiang, P. & Yang, R. Anisotropic thermal conductivity of 4H and 6H silicon carbide measured using time-domain thermoreflectance. *Mater. Today Phys.* **3**, 70–75 (2017).
25. Karmann, S., Helbig, R. & Stein, R. A. Piezoelectric properties and elastic constants of 4H and 6H SiC at temperatures 4–320 K. *J. Appl. Phys.* **66**, 3922 (1989).
26. Ye, W. N. & Xiong, Y. Review of silicon photonics: history and recent advances. *J. Mod. Opt.* **60**, 1299–1320 (2013).
27. Fan, T., Moradinejad, H., Wu, X., Eftekhar, A. & Adibi, A. High *Q* integrated photonic microresonators on 3C-SiC-on-insulator (SiCOI) platform. *Opt. Express* **26**, 25814–25826 (2018).
28. Cardenas, J. et al. Optical nonlinearities in high-confinement silicon carbide waveguides. *Opt. Lett.* **40**, 4138–4141 (2015).
29. Zheng, Y. et al. High-quality factor, high-confinement microring resonators in 4H-silicon carbide-on-insulator. *Opt. Express* **27**, 13053–13060 (2019).
30. Bracher, D. O., Zhang, X. & Hu, E. L. Selective Purcell enhancement of two closely linked zero-phonon transitions of a silicon carbide color center. *Proc. Natl Acad. Sci. USA* **114**, 4060–4065 (2017).
31. Song, B.-S. et al. High-*Q*-factor nanobeam photonic crystal cavities in bulk silicon carbide. *Appl. Phys. Lett.* **113**, 231106 (2018).
32. Radulaski, M. et al. Scalable quantum photonics with single color centers in silicon carbide. *Nano Lett.* **17**, 1782–1786 (2017).
33. Magyar, A. P., Bracher, D., Lee, J. C., Aharonovich, I. & Hu, E. L. High quality SiC microdisk resonators fabricated from monolithic epilayer wafers. *Appl. Phys. Lett.* **104**, 051109 (2014).
34. Lohrmann, A. et al. Integration of single-photon emitters into 3C-SiC microdisk resonators. *ACS Photon.* **4**, 462–468 (2017).
35. Song, B.-S. et al. Ultrahigh-*Q* photonic crystal nanocavities based on 4H silicon carbide. *Optica* **6**, 991–995 (2019).
36. Pelc, J. S. et al. Long-wavelength-pumped upconversion single-photon detector at 1,550 nm: performance and noise analysis. *Opt. Express* **19**, 21445–21456 (2011).
37. Rivoire, K. et al. Fast quantum dot single photon source triggered at telecommunications wavelength. *Appl. Phys. Lett.* **98**, 083105 (2011).
38. Dietrich, C. P., Fiore, A., Thompson, M. G., Kamp, M. & Höfling, S. GaAs integrated quantum photonics: towards compact and multi-functional quantum photonic integrated circuits. *Photon. Rev.* **10**, 870–894 (2016).
39. McCutcheon, M. W., Chang, D. E., Zhang, Y., Lukin, M. D. & Lončar, M. Broadband frequency conversion and shaping of single photons emitted from a nonlinear cavity. *Opt. Express* **17**, 22689–22703 (2009).
40. Wang, S. et al. 4H-SiC: a new nonlinear material for midinfrared lasers. *Photon. Rev.* **7**, 831–838 (2013).
41. Dory, C. et al. Inverse-designed diamond photonics. *Nat. Commun.* **10**, 3309 (2019).
42. Poshakinskiy, A. V. & Astakhov, G. V. Optically detected spin-mechanical resonance in silicon carbide membranes. *Phys. Rev. B* **100**, 094104 (2019).
43. Whiteley, S. J. et al. Spin–phonon interactions in silicon carbide addressed by Gaussian acoustics. *Nat. Phys.* **15**, 490–495 (2019).

Methods

4H-SiCOI preparation. A 100 mm wafer of on-axis, research-grade, high-purity semi-insulation (HPSI) 4H-SiC from Cree was diced into 10 mm × 10 mm dies. The dies were thoroughly cleaned and ~20 nm of thermal SiO_2 was grown. Separately, a SiO_2-on-Si handle wafer was prepared by thermal oxidation. The dies were bonded to the handle wafer at room temperature with manual pressure. The bond was strengthened by annealing at 900 °C, which resulted in a robust SiO_2–SiO_2 fusion bond. The wafer was then processed in a wafer grinder (DAG810, Disco) to thin the SiC to a thickness of 15 µm. The wafer was then chemically–mechanically polished (POLI-400L from G&P Tech.). Finally, the SiC film was further thinned to the desired thickness via reactive ion etching in SF_6/O_2 plasma (PlasmaTherm Versaline ICP). In an industrial setting, a final thickness variation of ~1 µm across a 100 mm wafer should be possible.

Fabrication of nanobeam PhC cavities. Starting with 4H-SiCOI with SiC thickness of 150 nm and buried SiO_2 thickness of 130 nm, we defined the PhC nanobeam pattern via electron-beam lithography (JEOL 6300-FS) in HSQ resist (FOx-16, Dow Corning). The pattern was transferred into the SiC via SF_6/O_2 plasma. The devices were suspended via a two-step undercutting process, where the buried oxide layer and the resist were etched in a vapour HF etch, followed by a XeF_2 gas etch to etch the Si, suspending the PhC cavity over 5 µm above the substrate. Because the residual density of V_{Si} in the nanobeam cavities was $\ll 1$ per cavity volume, we introduced them post-fabrication via flood implantation of H^+ with energy of 10 keV (CuttingEdge Ions) to generate a peak defect density at a depth of 75 nm, corresponding to the cavity mode maximum. The optimal fluence of 2.3×10^{10} cm^{-2} was estimated by assuming an energy-independent ratio between simulated[44] and measured[16] conversion efficiencies. No post-implantation annealing was performed.

High-*Q* ring resonator fabrication and characterization. Microring resonators were fabricated from 4H-SiCOI with SiC thickness of 350 nm and a buried SiO_2 thickness of 3 µm. As with the nanobeam cavities, HSQ resist was used. However, the only means of chemically removing the HSQ after the SiC etch is via HF, which would cause undesirable etching of the exposed buried oxide layer. To circumvent this issue, a 30 nm layer of PMMA resist was spun before spinning the HSQ resist. Subsequent lithography and etching were performed using the same steps as for the nanobeam PhC cavity fabrication. The HSQ was then lifted off by dissolving the PMMA layer in solvent. As a final step, we deposited 3 µm of SiO_2 cladding. Coupling to the ring resonators was carried out via two point-coupled waveguides (below critical coupling), terminated with inverse-designed grating couplers. The Mach–Zehnder interferometer used for spectral calibration of ring resonator measurements produced sinusoidal fringes with a free spectral range of 194.1 MHz, and the free spectral range was calibrated using an adaption of the radiofrequency spectroscopy method[45].

Data availability

All data relevant to the current study are available from the corresponding author on request.

References

44. Ziegler, J. F., Ziegler, M. D. & Biersack, J. P. SRIM—the stopping and range of ions in matter. *Nucl. Instrum. Methods Phys. Res. B* **268**, 1818–1823 (2010).
45. Li, J., Lee, H., Yang, K. Y. & Vahala, K. J. Sideband spectroscopy and dispersion measurement in microcavities. *Opt. Express* **20**, 26337–26344 (2012).

Acknowledgements

We thank S. Economou, W. Dong and R. Nagy for useful discussions. This research is funded in part by the Gordon and Betty Moore Foundation through grant no. GBMF 4743, the US Department of Energy, Office of Science, under award no. DE-SC0019174, and the National Science Foundation under grant number NSF/EFRI-1741660. Part of this work was performed at the Stanford Nanofabrication Facility (SNF) and the Stanford Nano Shared Facilities (SNSF), supported by the National Science Foundation under award no. ECCS-1542152. D.M.L. acknowledges support from the Fong Stanford Graduate Fellowship (SGF) and the National Defense Science and Engineering Graduate Fellowship. C.D. acknowledges support from the Andreas Bechtolsheim SGF and the Microsoft Research PhD Fellowship. M.A.G. acknowledges support from the William R. Hewlett SGF and the NSF Graduate Research Fellowship, and K.Y.Y. from the Nano- and Quantum Science and Engineering Postdoctoral Fellowship. S.D.M. acknowledges support from the Soheil and Susan Saadat Graduate Fellowship. M.R. acknowledges support from the Nano- and Quantum Science and Engineering Postdoctoral Fellowship. G.H.A. acknowledges support from the STMicroelectronics SGF and Kwanjeong Educational Foundation Fellowship. R.T. acknowledges funding from Kailath SGF.

Author contributions

D.M.L., C.D., M.A.G. and J.V. conceived the experiment. D.M.L. and C.D. developed the material platform and the fabrication techniques. C.D., D.M.L., S.D.M., G.H.A. and S.S. conducted the quantum experiments. M.A.G., D.M.L., K.Y.Y. and C.D. performed nonlinear experiments. R.T., D.M.L. and M.R. performed cavity design and analysis. D.V. performed inverse design simulations. J.V. supervised the project. All authors discussed the results and contributed to the final manuscript.

Competing interests

The authors declare no competing interests.

Additional information

Supplementary information is available for this paper at https://doi.org/10.1038/s41566-019-0556-6.

Correspondence and requests for materials should be addressed to J.V.

Reprints and permissions information is available at www.nature.com/reprints.